Computation of the noise of initially laminar jets using a statistical approach for the acoustic analogy: application and discussion

Sergey Karabasov, Christophe Bogey, Tom Hynes

Computation of the noise of initially laminar jets using a statistical approach for the acoustic analogy: application and discussion

Sergey A. Karabasov[1],
Whittle Laboratory, University of Cambridge Department of Engineering, Cambridge, CB3 0DY, UK

Christophe Bogey[2]
Laboratoire de M´ecanique des Fluides et d'Acoustique, 69134 Ecully, France

and

Tom Hynes[3]
Whittle Laboratory, University of Cambridge Department of Engineering, Cambridge, CB3 0DY, UK

The details of the sound sources within two initially laminar jets that correspond to different inflow conditions, one fully laminar and the other with nozzle boundary layer forcing, are studied using an acoustic analogy. The source statistics are generated from Large Eddy Simulations and some issues associated with the practicalities of doing this and the frequency and lengthscale ranges of validity that one can expect from such simulations are explored. The comparative importance of various source terms confirms the results of previous studies with the exception of one extra term. Reasonable agreemeent is found between noise predictions using the acoustic analogy with that of a previously-conducted LES-ILEE control surface method, over the frequency range of validity. The acoustic analogy is used to determine the lengthscales which contribute to noise at different radiated angles to the jet and where they are located in the jets.

I. Introduction

Initially laminar jets originating from a round nozzle were the subject of a Large-Eddy Simulation (LES) study by Bogey and Bailly (2010). Several isothermal axi-symmetric jets were considered to investigate the effects of the nozzle-exit conditions on the flow and sound fields. The differing nozzle-exit conditions, which were inlet conditions for the calculation through the jet, led to noticeably different shear layer behaviour. This in turn led to differences in the far-field sound, as predicted using an approach in which the Linearised Euler Equations (LEE) were coupled to the LES solution at an open cylindrical surface outside of the jet.

Goldstein (2003) developed a generalized acoustic analogy formulation for jet noise in which the propagation of noise is modelled using the Linearised Euler Equations and the corresponding source description involves fourth order correlations of turbulence properties. A development of this method was used by Karabasov et al (2010) to model these statistics through a combination of processed LES data and the prediction of length and timescales based on RANS calculations. This work highlighted the dominance of a few of the fourth order correlations and provided some evidence of the way such statistics could be modelled and scaled using the RANS predictions. The sound predictions of that paper showed encouraging agreement with measurements.

The work described in this paper attempts to apply the formulation described in Karabasov et al (2010) to two of the jets for which calculations were performed by Bogey and Bailly (2010). One aim of this paper is to perform a more detailed test of the assumptions underlying the scaling of terms using the acoustic analogy method described in Karabasov et al (2010). The second aim is to examine whether the formulation described in Karabasov et al (2010) is robust enough to distinguish between the different cases described in Bogey and Bailly (2010) in terms of the

[1] Royal Society University Research Fellow, Engineering Department, 1 JJ Thompson Avenue, Sr AIAA Member.
[2] CNRS Scientist, Department Name, UMR CNRS 5509, Ecole Centrale de Lyon, AIAA Member.
[3] Reader in Mechanical Engineering, Engineering Department, 1 JJ Thompson Avenue, AIAA Member

predicted far-field sound. In order to avoid any issues associated with how well RANS methods could predict the flow in these jets and for increased integrity of the acoustic analogy method, no RANS calculation will be used but all mean flow properties and statistics of the turbulence will be extracted from the LES calculations. The final aim is to attempt to explain further how the changes in nozzle-exit conditions produce the calculated effect on far-field sound and to explore how various approximations made in the propagation methodology and the source statistics modelling used in the approach of reference Karabasov et al (2010) affect the predicted sound.

II. Jet Properties and LES Details

The jets studied by Bogey and Bailly (2010) are isothermal, have a Mach Number of 0.9 and have a Reynolds Number of 10^5 based on nozzle diameter. They issue from a short pipe nozzle (length/r_0 = 1.1, where r_0 is the nozzle exit radius) which had Blasius boundary layer velocity profiles of varying thicknesses imposed at nozzle inlet. The paper discussed in detail a variety of initial boundary layer thicknesses and two cases for which a random forcing was applied within a section of the nozzle boundary layer in order to trip the boundary layer on the inside of the nozzle. In general, the results reported successfully predicted the effects of the nozzle exit boundary layer thickness and also that of the boundary layer tripping on noise, in agreement with those observed in laminar jet noise experiments by Zaman and Hussain (1980) and Zaman (1985) (Fig.1)

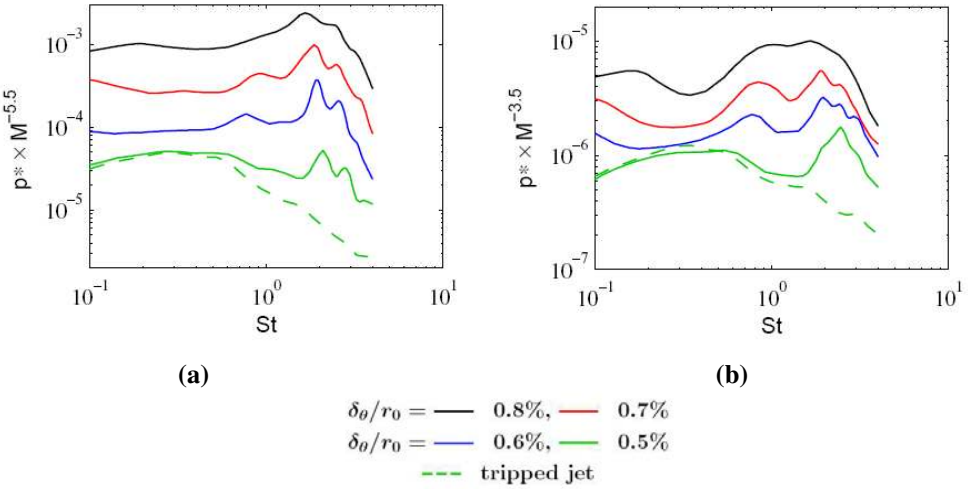

Figure 1. Measured far-field sound spectra for laminar jets of different boundary layer nozzle thicknesses (a) at 30^0 angle and (b) 90^0 (Zaman, 1985).

The two particular jets considered in this paper correspond to those with a shear layer thickness of 0.05 r_0 (momentum thickness of 0.0056 r_0). One of the jets has a fully laminar inflow condition (refered to as "untripped"), with any unsteadiness generated as a self-sustaining part of the LES solution after the withdrawal of an initial short period of seeded unsteadiness. The other has a random forcing unsteady pressure amplitude 2000 Pa imposed over an internal section of the nozzle (0.2-0.4 r_0). This results in what Zaman (1985) described as nominally laminar and we shall refer to as "tripped". The two jets have similar initial peak root-mean-square (r.m.s.) axial velocity values: below 1% of the jet velocity for the untripped case, and around 1.9% for the second, tripped jet. The potential core length of the tripped jet is 9 jet diameters and that of the untripped one is 7. As shown by Bogey and Bailly, this difference in the inflow conditions, that is insignificant in comparison to the mean flow quantities, can lead to 5-10dB change in the peak sound levels. A major acoustic mechanism identified in the two jets is thought to be associated with vortex pairing which Bogey and Bailly identified as having a characteristic frequency St=2.16 and St=1.61 for the tripped and untripped jets respectively, where the Strouhal number St is based on the jet diameter. Bogey and Bailly (2010) also show that the vortex pairing event at the lip-line location happens around z=0.45 for the tripped jet and at z=0.8D for the untripped one.

The LES calculation domain used by Bogey and Bailly is terminated at the downstream end by a sponge zone starting at approximately 12.6 jet diameters from the nozzle exit. Their acoustic predictions were obtained by matching the LES solutions to an Isotropic Linearised Euler Equations (ILEE) model. The ILEE solution started

from an open control surface, which covered the axial domain extent at a distance of 2.6 jet diameters from the jet axis.

In the present paper, a method based on the generalised acoustic analogy of Goldstein (2003) is used based on statistics reprocessed from unsteady solution data stored at the time of the initial Bogey and Bailly calculations. The aims of the original paper were to study the initial shear layer development and subsequent evolution of the early part of the jet. Because of this, the unsteady solution stored was tailored to that purpose and has some limitations for the purposes of this paper. The two sets of LES data for the tripped and untripped jet are available only in one jet symmetry plane and at one cylindrical surface (at the lip-line location). The grid density corresponds to the original 595 × 256 × 249 LES calculation. The spatial spread of the data available in the symmetry plane is 12.5 jet diameters axially and 1 jet diameter radially. The data sampling rate is $\Delta t = 0.05\, D/U$ and 4307 time samples in total are available for acoustic post-processing. A schematic of the computational setup of the problem is shown in Fig.2. Because of the limited LES fields in the circumferential direction, most of the acoustic analogy modelling will be restricted to analysis using the in-plane data. The correlation lengthscale for variations in the circumferential and radial direction will, at each position in the jet, be assumed to be the same as that derived for variations in the axial direction, as in Karabasov et al (2010). The study of the effect of correlation lengthscale anisotropy on noise will be a subject of the future publication.

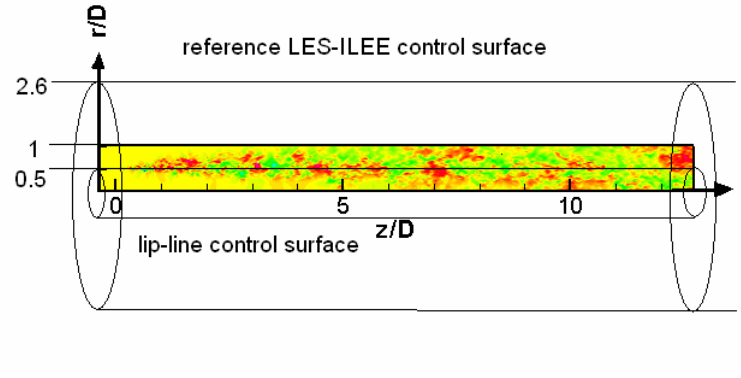

Figure 2. Input LES data definition delineating the area available for the acoustic analogy source estimation, the control surface location of the reference LES-ILEE is also shown.

Fig. 3 shows typical instantaneous snap shots of velocity fluctuations computed from the LES-data fields in the symmetry plane of the two jets. For better visibility, an axis ratio 1:10 (axial versus radial) is used here and throughout the rest of the paper. Black lines correspond to a nominal location of the jet edges. The inward travelling line is relatively easy to position. The outer one is more problematical and should be regarded as indicative only because of the large excursions from the mean here. One observation to make here is that the instantaneous velocity fields of the two very different jets look similar in the first 10 diameters. There are notable velocity oscillations across the edge of the jet and what looks like large-scale structures convecting downstream in both cases. If there wasn't a slight difference in the end of jet potential core location, these flow snapshots could even be regarded as different realisations of the same turbulent flow.

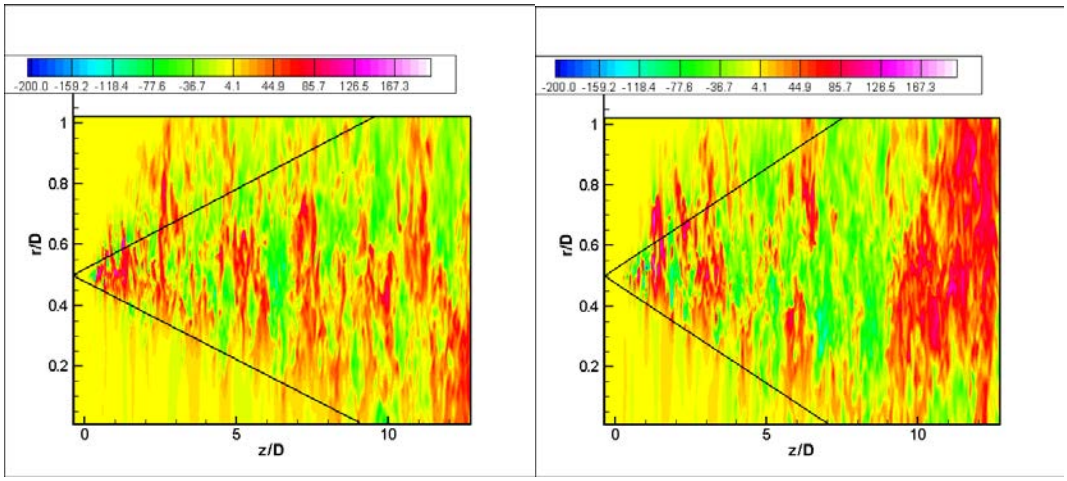

(a) **(b)**

Figure 3. Velocity fluctuations in (a) tripped jet (potential core ending after approximately 9 jet diameters) and (b) untripped (potential core ending after approximately 7 jet diameters).

III. Acoustic Analogy Modelling

The acoustic analogy used in this study follows the formulation described in Karabasov et al (2010). The following system of Adjoint Linearised Euler Equations (LEE) in the Goldstein (2003) formulation is used:

$$\begin{aligned}
&\frac{\partial \rho'}{\partial \tau}+\frac{\partial}{\partial y_j}(\rho' \tilde{v}_j + u_j) = 0 \\
&\frac{\partial u_i}{\partial \tau}+\frac{\partial}{\partial y_j}(\tilde{v}_j u_i)+\frac{\partial p'}{\partial y_i}+u_j \frac{\partial \tilde{v}_i}{\partial y_j}-\left(\frac{\rho'}{\bar{\rho}}\right)\frac{\partial \tilde{\tau}_{ij}}{\partial y_j}=\frac{\partial T'_{ij}}{\partial y_j} \quad i=1,..3. \\
&\left(\frac{1}{\gamma-1}\right)\frac{\partial p'}{\partial \tau}+\left(\frac{1}{\gamma-1}\right)\frac{\partial}{\partial y_j}(p' \tilde{v}_j)+\frac{\partial}{\partial y_j}(u_j \tilde{h})+p'\frac{\partial \tilde{v}_j}{\partial y_j}-\left(\frac{u_i}{\bar{\rho}}\right)\frac{\partial \tilde{\tau}_{ij}}{\partial y_j}=0.
\end{aligned} \tag{1}$$

The right-hand side of these equations is the fluctuating Reynolds stress sources, which are the sources that survive after rearrangement of the Navier-Stokes equations for isothermal jets. The far-field sound predicted using this model is given by a convolution integral of the adjoint LEE Green's function tensor $\hat{I}_{ij}$ with the tensor of fourth-order two-space two-time velocity correlation function

$$\hat{P}(\mathbf{x},\omega)=\int\limits_{V_\infty(\mathbf{y})}\int_{\mathbf{\Delta}}\hat{R}_{ijkl}(\mathbf{y},\mathbf{\Delta},\omega)\hat{I}_{ij}(\mathbf{y},\omega\,|\,\mathbf{x})\hat{I}_{kl}(\mathbf{y}+\mathbf{\Delta},-\omega\,|\,\mathbf{x})\,d^3\mathbf{\Delta}d^3\mathbf{y} \tag{2}$$

The velocity correlation coefficients $\hat{R}_{ijkl}(\mathbf{y},\mathbf{\Delta},\omega)$ are obtained by time-averaging the unsteady LES solutions, where Favre-averages for the fluctuating quantities are used. The previous study showed that the corresponding fourth-order correlation coefficients $\hat{R}_{ijkl}(\mathbf{y},\mathbf{\Delta},\omega)=\int R_{ijkl}(\mathbf{y},\mathbf{\Delta},\tau)e^{-i\omega\tau}\,d\tau=\int\overline{T'_{ij}(\mathbf{y},t)T'_{kl}(\mathbf{y}+\mathbf{\Delta},t+\tau)}e^{-i\omega\tau}\,d\tau$ in a number of acoustically important jet regions (e.g, end of potential core, developed shear layer region) can be well approximated by an analytical Gaussian function characteristised by amplitude, length and time scales

$$R_{ijkl}(\mathbf{y},\mathbf{\Delta},\tau)=A_{ijkl}(\mathbf{y})\exp[-\Delta_1/(\tilde{v}_1\cdot\tau_s(\mathbf{y}))-\ell n2\left((\Delta_1-\tilde{v}_1\cdot\tau)^2/l^2_{sz}(\mathbf{y})+\Delta^2_2/l^2_{s\theta}(\mathbf{y})+\Delta^2_3/l^2_{sr}(\mathbf{y})\right)]. \tag{3}$$

In the present work, these scales are computed from the LES data at every point of the jet symmetry plane where data is available, which region is as sketched in Fig. 2. In contrast to the original paper by Karabasov et al (2010), the present work does not use a RANS interpolation step, which involves evaluating the lengthscales at selected points in the jet and then assuming that they vary in the same way as lengthscales and timescales as predicted by a RANS method.

The method of computing the adjoint Green's function has been slightly modified in comparison with the work of Karabasov and Hynes (2006). As before, the governing system of adjoint LEE are solved in the frequency domain in the cylindrical-polar coordinate system $(y_1, y_2, y_3) = (x, r, \theta)$, $(x_1, x_2, x_3) = (x_o, r_o, \theta_o)$ are given by

$$\mathbf{L}^* \mathbf{G}_n^s = \begin{pmatrix} i\omega\rho_n + \bar{u}\frac{\partial}{\partial x}\rho_n + \bar{v}\frac{\partial}{\partial r}\rho_n & + \frac{1}{\bar{\rho}}\left(u_n \frac{\partial}{\partial y_\alpha}\bar{\tau}_{xy_\alpha} + v_n \frac{\partial}{\partial y_\alpha}\bar{\tau}_{ry_\alpha}\right) \\ i\omega u_n + \bar{u}\frac{\partial}{\partial x}u_n + \gamma\frac{\bar{p}}{\bar{\rho}}\frac{\partial}{\partial x}p_n & + \bar{v}\frac{\partial}{\partial r}u_n + \frac{\partial}{\partial x}\rho_n - u_n\frac{\partial}{\partial x}\bar{u} - v_n\frac{\partial}{\partial x}\bar{v} + (\gamma-1)\frac{p_n}{\bar{\rho}}\frac{\partial}{\partial y_\alpha}\bar{\tau}_{xy_\alpha} \\ i\omega v_n + \bar{u}\frac{\partial}{\partial x}v_n + \gamma\frac{\bar{p}}{\bar{\rho}}\frac{\partial}{\partial r}p_n - u_n\frac{\partial}{\partial r}\bar{u} & + \bar{v}\frac{\partial}{\partial r}v_n + \frac{\partial}{\partial r}\rho_n - v_n\frac{\partial}{\partial r}\bar{v} + (\gamma-1)\frac{p_n}{\bar{\rho}}\frac{\partial}{\partial y_\alpha}\bar{\tau}_{ry_\alpha} \\ i\omega w_n + \bar{u}\frac{\partial}{\partial x}w_n - \gamma\frac{\bar{p}}{\bar{\rho}}\frac{n}{r}p_n & + \bar{v}\frac{\partial}{\partial r}w_n - \frac{n}{r}\rho_n - \frac{\bar{v}}{r}w_n \\ \underbrace{i\omega p_n + \bar{u}\frac{\partial}{\partial x}p_n + \frac{\partial}{\partial x}u_n + \frac{1}{r}\frac{\partial}{\partial r}(rv_n)}_{\text{Locally parallel jet meanflow terms}} & + \bar{v}\frac{\partial}{\partial r}p_n + \frac{n}{r}w_n - (\gamma-1)p_n\left(\frac{\partial}{\partial x}\bar{u} + \frac{1}{r}\frac{\partial}{\partial r}(r\bar{v})\right) \end{pmatrix} = 0, \quad (4)$$

where $\mathbf{G}^s = \sum_{n=0}^{\infty} \mathbf{G}_n{}^s = \sum_{n=0}^{\infty} (\rho_n{}^s \cos\theta', u_n{}^s \cos\theta', v_n{}^s \cos\theta', w_n{}^s \sin\theta', p_n{}^s (\gamma-1)\cos\theta')^T$,

$\theta' = n(\theta - \theta_o)$ is the circumferential angle in the jet with respect to the observer location, and ρ_n^s, (u_n^s, v_n^s, w_n^s), p_n^s are the adjoint density, velocity and pressure variables per mode in a cylindrical-polar coordinate system.

This system is augmented by the corresponding reciprocal boundary conditions that correspond to a point sink at the observer location. In contrast to the case studied by Karabasov and Hynes (2006), in this current study the domain for the propagation calculation does not include the nozzle lip geometry. Instead, non-reflecting boundary conditions of characteristic-type with a sponge buffer layer are used at all open boundaries. The computational domain for the propagation calculation is extended upstream of the nozzle exit as a parallel jet flow taking the flow profile at the jet nozzle exit. This extension is implemented as a non-reflecting sponge zone that spans over several jet diameters. A further slight variation, that improves the conditioning of the calculation procedure, is that the solution is found as a scattered wave component $\mathbf{G}^s = \mathbf{G} - \mathbf{G}^{locally\ parallel}$, relative to the Green's function that corresponds to the solution of the locally parallel jet wave scattering problem (which is found from the solution of a straightforward set of ordinary differential equations). The method outlined in Karabasov and Hynes (2006) uses a scattered component relative to a free space solution.

The main advantage of choosing to find the solution as a difference from the locally parallel solution is that the sponge zones exhibit a numerically superior non-reflecting property when compared with those which sponge towards a solution with no jet. The numerical methodology has been validated against model problems and its detailed description will be a subject of the future publication.

IV. Acoustic post-processing of the LES data

For each position in the jet for which LES data is available, the fourth-order velocity correlations are first computed.

$$R_{ijkl}(\mathbf{y}, dx, dt) = \overline{\rho(\mathbf{y}+dx, \tau+dt) v_i''(\mathbf{y}+dx, \tau+dt) v_j''(\mathbf{y}+dx, \tau+dt) \rho(\mathbf{y}, \tau) v_k''(\mathbf{y}, \tau) v_l''(\mathbf{y}, \tau)} -$$
$$\overline{\rho(\mathbf{y}+dx, \tau+dt) v_i''(\mathbf{y}+dx, \tau+dt) v_j''(\mathbf{y}+dx, \tau+dt)} \cdot \overline{\rho(\mathbf{y}, \tau) v_k''(\mathbf{y}, \tau) v_l''(\mathbf{y}, \tau)}$$

Here i,j,k,l=1,2,3 are local Cartesian directions aligned with 1 – axial, 2 – circumferential and 3 radial directions of the cylindrical-polar coordinate system. The next step is to find a fit to this numerical data using the analytical Gaussian function (3). The choices to be made at this step are important for the model performance and, for this reason, it is described below in some detail.

A. Fitting the velocity correlation coefficients to an analytical Gaussian shape

The calculation of the scales in the axial direction is considered first, which corresponds to letting $\Delta_1 = dx, \Delta_2 = \Delta_3 = 0$ in (3). A four-step procedure for computing the correlation fits is used as follows:

- Local maxima for the Gaussian are calulated from the numerical $R_{ijkl}(\mathbf{y}, dx, dt)$; if the local maxima are not positive the correlation fit is flagged as failing;
- Assuming the magnitude of the correlation peak decays with spatial separation, the numerical value which is approximately 60% of the magnitude of the autocorrelation amplitude $R_{ijkl}^{(60\%\,peak)} \sim 0.6 A_{ijkl}(\mathbf{y})$ and its corresponding separation in time $\tau_{peak} = dt = \Delta_1 / \tilde{v}_1$ are considered, and the correlation time based on the 60% values is computed $\tau_s(\mathbf{y}) = \tau_{peak} / \log(A_{ijkl}(\mathbf{y}) / R_{ijkl}^{(60\%\,peak)})$; if this correlation time is not positive for positive spatial separations the correlation fit is flagged as failing;
- The correlation velocity based on the local 60% peak values is computed, $\tilde{v}_1 = \Delta_1 / dt$; from the characteristic width $\Delta t^{(width)}$ of the 60% profile that corresponds to the amplitude decay from $R_{ijkl}^{(60\%\,peak)} = R_{ijkl}^{(60\%\,peak)}(0)$ to $R_{ijkl}^{(60\%\,peak)}(\Delta t^{(width)})$ the length scale is computed $l_{sz}(\mathbf{y}) = \sqrt{Log(2)\left(\tilde{v}_1 \cdot \Delta t^{(width)}\right)^2 / Log(R_{ijkl}^{(60\%\,peak)}(0) / R_{ijkl}^{(60\%\,peak)}(\Delta t^{(width)}))}$.

Once the axial correlation values are calculated they are substituted to (3) and the correlation lengths in the remaining two spatial directions are calculated in a similar manner.

B. Regions of validity of Gaussian Fits

The above procedure has been applied to the data for the tripped and untripped jets. In general, the more time samples that are taken for averaging, the more statistically converged the LES data become, and the bigger the area of the jet that satisfies the criteria for the Gaussian fit model (Fig4).

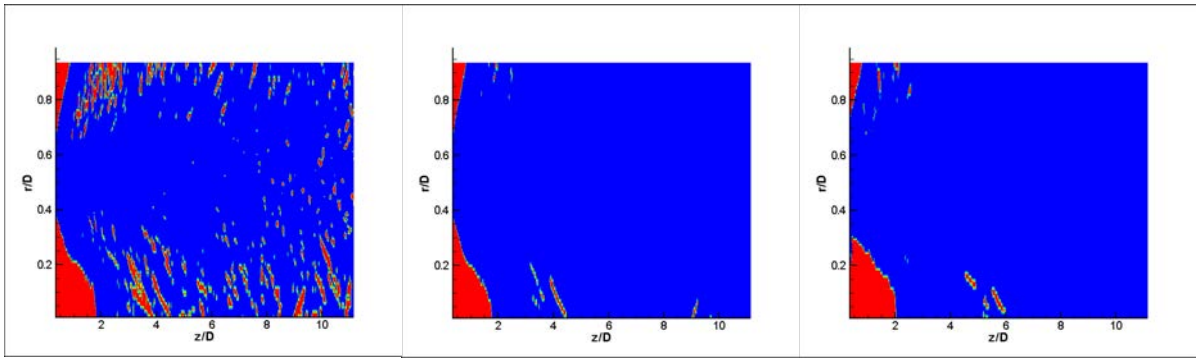

(a) **(b)** **(c)**

Figure 4. Improving the statistical convergence of LES data with bigger number of time samples, areas of the domain where the correlation fit works are blue and red when it fails (a) for 25-50% time samples and (b) 100% time samples for the untripped jet, (c) 100% time samples for the tripped jet.

The locations where the fit fails even when using the full 100% of the time samples available falls into two categories. The first is most typical of the upstream parts of the jet and also for the outer side of the shear layer (Fig5a). Most of these locations disappear when the number of time samples is increased from 25% to 100%, implying a probable lack of numerical-LES-data convergence. The second category is typically in the region towards the end of the potential core and on the inner side of the developed shear layer as it intrudes into the jet core. This can be associated with growing and decaying waves (Fig5b) and most of these location survive the transition from 25% to 100% data sampling. The correlation amplitudes of the miss-fits of both categories are typically 2-5 orders of magnitude smaller than the peak correlation amplitudes in the jet shear layer.

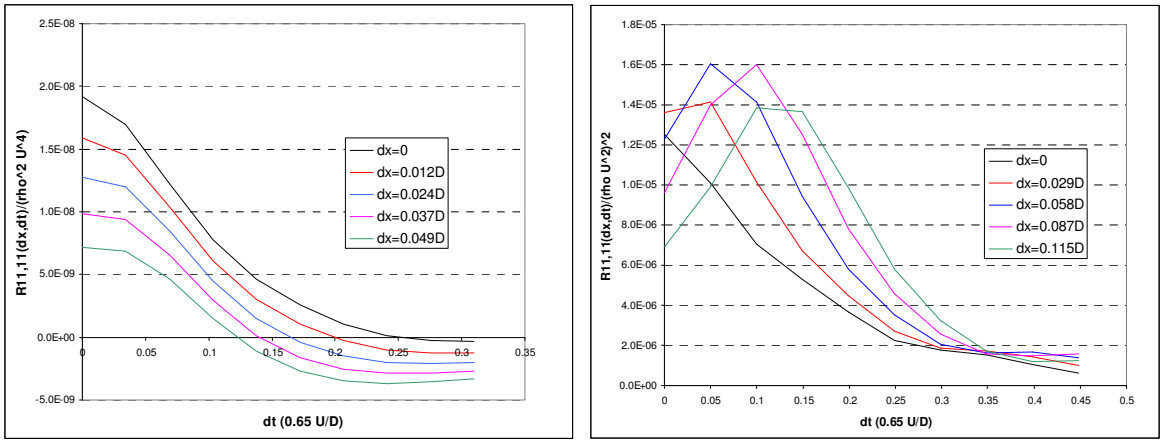

(a) **(b)**

Figure 5. Typical cases of the fourth-order correlation coefficients not well fitted by decaying Gaussian shape: (a) in the shear layer location at z=0.5D and (b) close to the jet centre line at z=4D.

Fig.6a shows how well the correlation fits work in the jet shear layer locations (z=4D, r=0.5D). As the distance from the nozzle exit increases, a slow-down in the LES data convergence is noted. This is seen as stagnation of the zero-space-separation curve that, for big separation times, asymptotes towards some positive value (z=8D, Fig.6b). The same trend is also observed for the outer radial jet locations. In the right and top 20% areas of the jet, that correspond to z ~ 9-12D axially and r ~ 0.8-1D radially, this stagnation value is more than 10% of the peak correlation amplitude. This suggests that the LES data in the boundary regions of the jet are probably not well converged for the low frequencies that correspond to the tail of the correlation distribution.

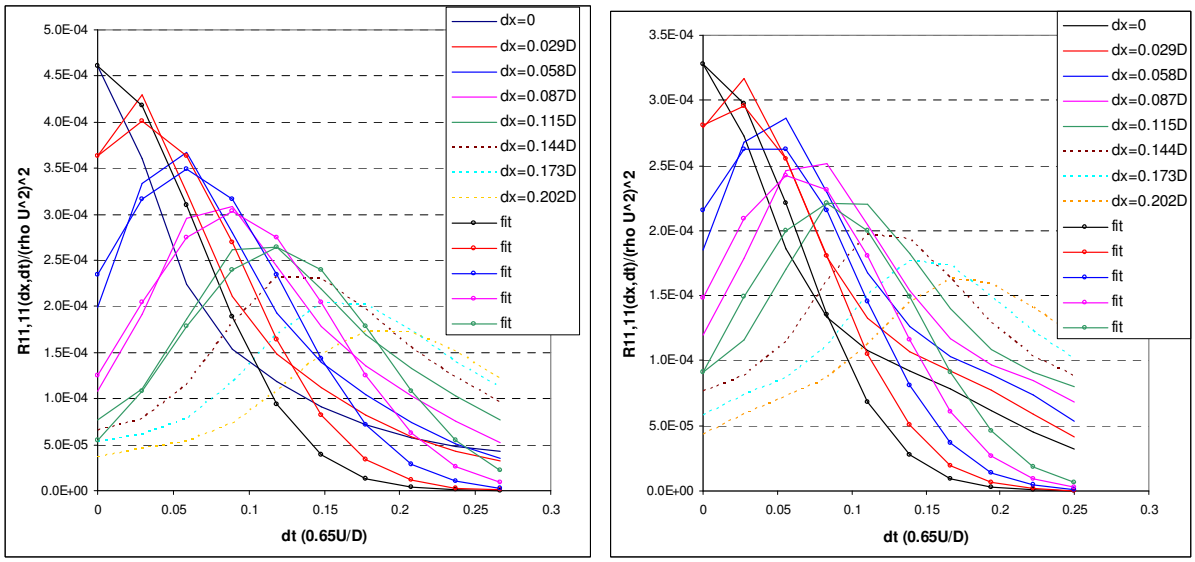

(a) **(a)**

Figure 6. Correlation coefficients and Gaussian fits for the tripped jet in the shear layer location r=0.5D at (a) z=4D and (b) z=8D.

Another challenging location for the correlation fits is close to the inner edge of the shear layer, which, despite a relatively small correlation amplitude, is distributed over a large area, hence, can be potentially important for noise estimates. In these locations the shear layer protrudes intermittently into the jet potential core which creates regions of large differences in scales over a relatively small area in the jet. Fig.7 shows examples of correlation coefficients in two jet locations where the correlation lengths vary by a factor of 2-3 over two jet diameters, as does the correlation time. Interestingly, the Gaussian fit model works rather well for both these jet locations.

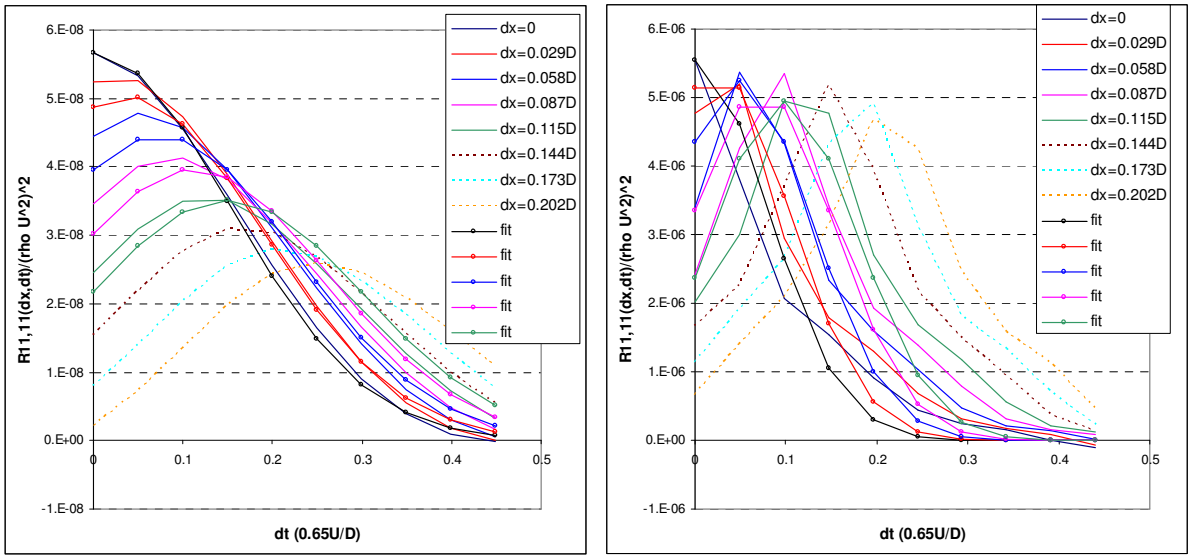

(a) **(b)**

Figure 7. Correlation coefficients and Gaussian fits in the tripped jet at the same r=0.1D, (a) z=3D and (b) z=5D.

C. Correlation fit map

For future reference, it is useful to draw a schematic of the regions of the jet where the Gaussian correlation fit appears to work well and where the fits are dubious and where they fail completely. Fig.8 shows such a schematic for the tripped case.

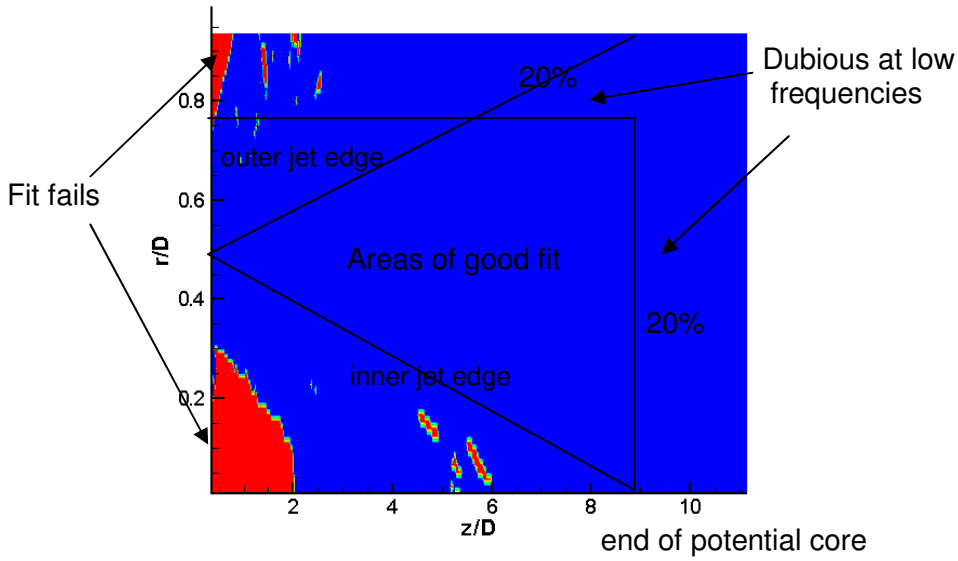

Figure 8. Schematic of the correlation fits for the tripped jet case.

The above information can be used to assess the limits of applicability of the overall acoustic analogy model for the tripped jet case that bears some similarities with the solutions obtained for a turbulent JEAN case (at higher Re = 10^6) considered in Karabasov et al (2010), and in Power et al (2004). Fig.9 shows the efficiently radiating (i.e. when

weighted with the propagation term $\hat{I}_{ij}\hat{I}_{kl}$ in equation (2)) acoustic source distribution of the JEAN model at 30^0 relative to the downstream jet direction for St=0.2 and St=1. Given the present LES data limitations that is effectively bracketed by z~9D in the axial direction for low frequencies, it is reasonable to expect that the low frequency end of the applicability of the acoustic noise prediction for the current study falls in between 0.2 <St <1 .

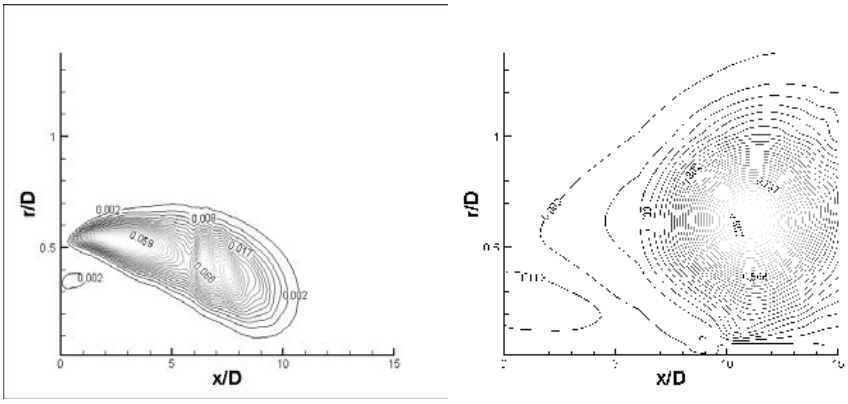

(a) **(b)**

Figure 9. Efficient acoustic source distribution for the turbulent JEAN case at 30^0 observer location from Karabasov at al (2010) for (a) St=1 and (b) St=0.2.

V. Acoustic source scales

Fig.10 a,b show the results for the autocorrelation scale distribution for the tripped and untripped jets for the largest noise source component R_{1111}. Fig10c shows the corresponding lip-line profile. Also marked are the locations of shear-layer vortex pairing events as found and discussed by Bogey and Bailly(2010).

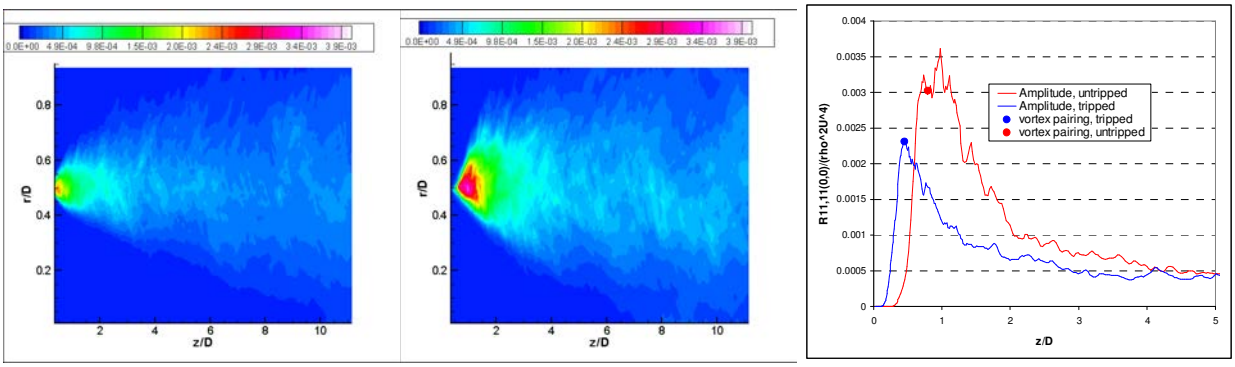

(a) **(b)** **(c)**

Figure 10. Autocorrelation field of the longitudinal component (R_{1111}) for (a) tripped jet, (b) untripped jet and (c) the lip-line distributions for the two jets, vortex pairing locations from Bogey and Bailly (2010) are shown.

Fig.11 shows the lip-line distributions of autocorrelation amplitudes normalised by the longitudinal component R_{1111}. For improving convergence, circumferential averaging is applied (this radial location is the only one where data is available to do this). For the untripped jet, there is a notable amplification of the two correlation components that lie in the normal plane at the upstream end of the jet which may be associated with the initial development of the laminar shear layer. Apart from this effect of the laminar inflow condition, the relative amplitudes of the two jets further downstream are similar. In comparison with the previously studied fully turbulent jet case in Karabasov et al (2010), here there is a relatively stronger contribution from the normal plane correlation components (R_{2222}, R_{3333}).

These are exactly the same set of terms that were found to be dominant by Karabasov et al (2010), with the one exception of a new non-small term that is associated with the axial-radial velocity interaction (R_{1112}).

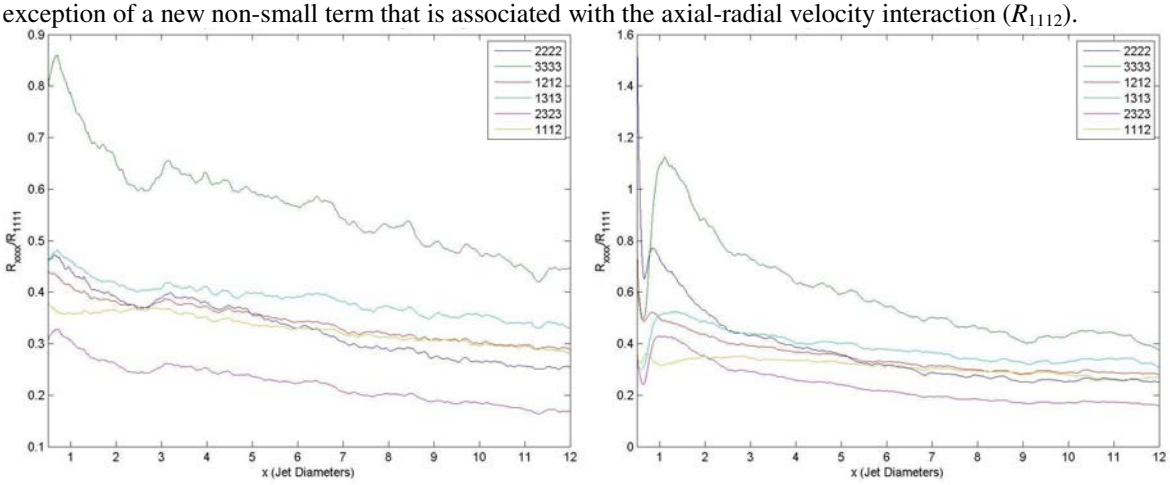

(a) **(b)**

Figure 11. Relative amplitude distribution for the most significant source components for (a) tripped jet and (b) untripped.

The correlation length scales in the axial, radial and circumferential direction along the lip line of the two jets are shown in Fig 12. The uneven character of the correlation curves is associated with insufficient averaging time. There is a prominent amplification of the scales at the upstream end in the case of untripped jet, which is associated with the laminar inflow boundary condition for this case. Apart from the peak at the beginning of the jet in the untripped case, the scales of both jets look similar. It is interesting to note that the relative scale values (axial length scale to radial scale is approximately 3 to 1 and circumferential scale to radial scale is approximately 3 to 2) of these initially laminar jets, in good agreement with the values found experimentally on the lip line location of a round jet experiment by Morris and Zaman (2010).

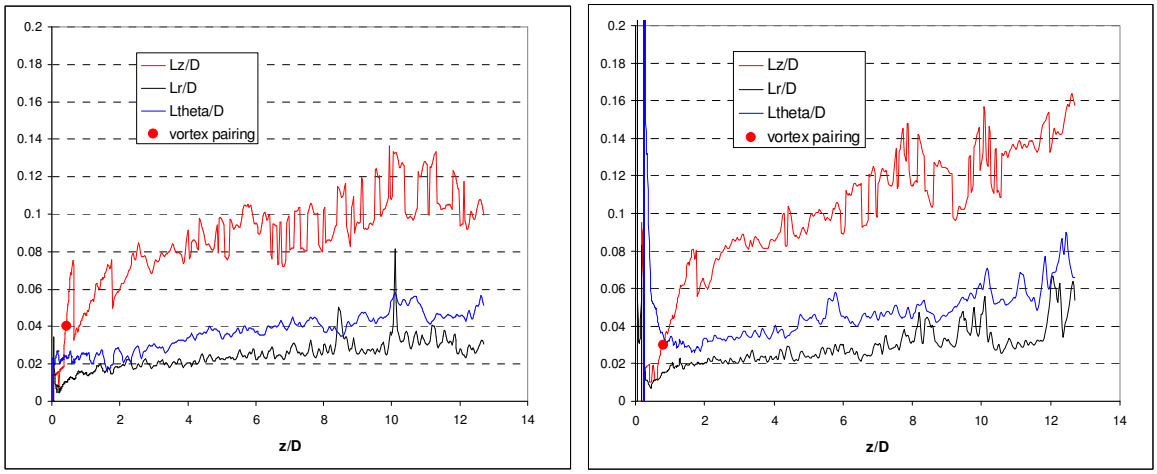

(a) **(b)**

Figure 12. Correlation length scales along the lip line for (a) tripped jet and (b) untripped; locations of vortex pairing from Bogey and Bailly (2010) are also shown.

The lip-line correlation timescale distribution for the tripped jet is shown in Fig.13a. The distribution for the untripped case is similar and not shown. The non-smooth nature of the length distribution curves is due to the insufficient sample averaging. When averaged circumferentially, which can be performed at this particular radial location, the curves become much smoother as depicted in fig 13b.

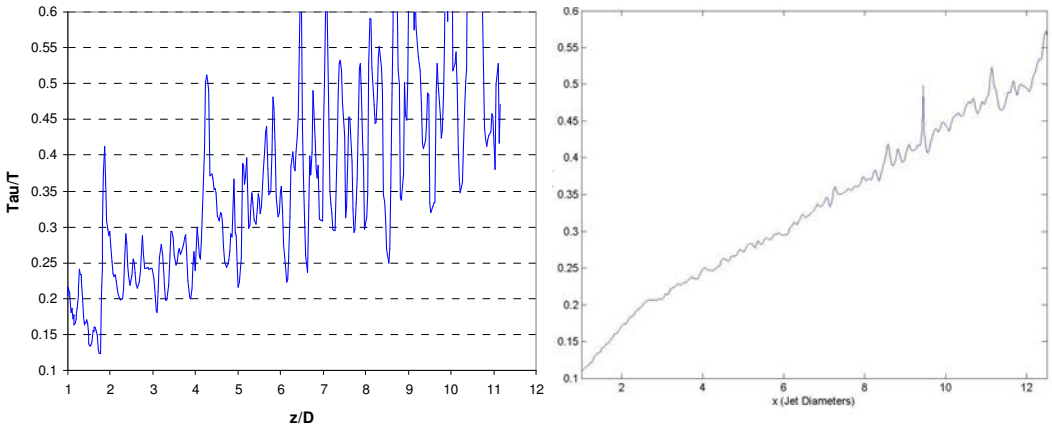

(a) **(b)**

Figure 13. Correlation time scales along the lip line for (a) the tripped jet in-plane and (b) the same after circumferential averaging.

The spatial distribution of the axial correlation scales for both jets in the symmetry plane is shown in Fig.14. The contours are chosen to highlight the correlation scales which contain most of the acoustic source. The correlation scales tend to grow with downstream and radial distance with the jets. There is a region of large scales emerging around the inner edge of the jets, which then decay with further downstream distance (cf Fig.7). The region of the large spatial scales is more prominent for the tripped jet which has a larger potential core.

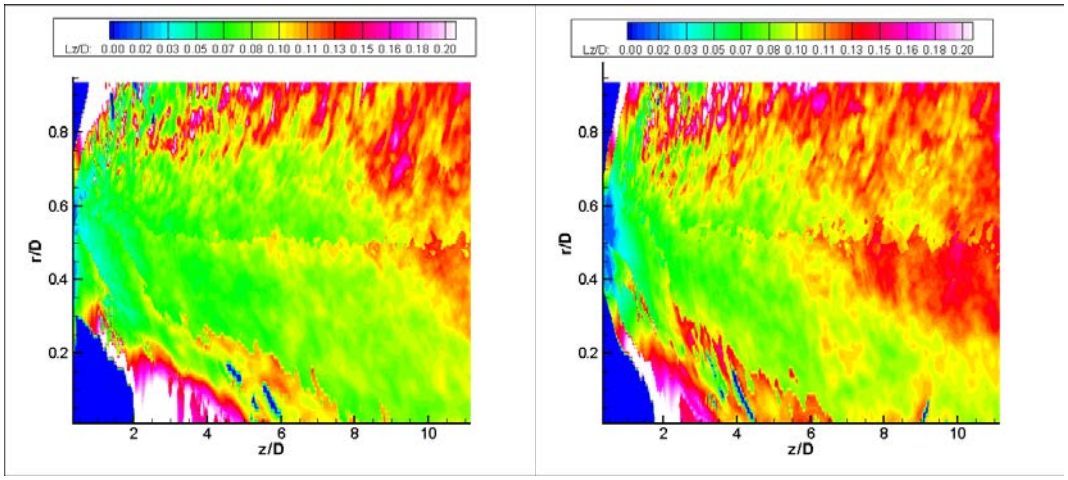

(a) **(b)**

Figure 14. Axial correlation length scales for (a) tripped jet and (b) untripped.

VI. Acoustic prediction results and consistency checks

Fig.15 shows the predicted sound Power Spectral Density (PSD) [dB/St] for the two jets at 30^0 and 90^0 to the downstream axis. The observer location is at 30 jet diameters from the nozzle exit. The acoustic analogy prediction is based on the solution of the linearised Euler equations (1) and the statistical source model that includes all the major terms in addition to the longitudinal one, with the integral evaluated over the entire region for which there is LES data. The spectra of the reference solutions obtained with the open control surface LES-ILEE method from Bogey and Bailly (2010) are shown in the same plots for comparison. For both angles to the jet and for a wide range of frequencies, 0.5<St<6 the prediction of the two methods are within 1-2dB the tripped jet. For the untripped jet, the agreement between the two methods is less good and amounts to 3-4dB. For this case, the under prediction of peak noise by the acoustic analogy method in comparison with the reference LES-ILEE solution is likely to be

caused by a very strong vortex-pairing identified by Bogey and Bailly (2010). For the untripped jet, the vortex pairing is located further downstream and closer to the edge of the jet, when compared with the tripped case. This location may be less amenable to statistical averaging because of the greater excursions from the mean here.

There are also some differences between the two predictions for both jets at high and low frequencies. The high-frequency discrepancy is caused by the grid cut-off frequency, above St=6, imposed by the grid resolution at the LES-ILEE control surface location. The discrepancies for low frequencies, St<0.5 between the two predictions are probably associated with insufficient time averaging and with the reduced extent of the spatial LES domain, as discussed in Section II, and also possibly by the numerical artifacts of the open-surface LES-ILEE method. The latter is acknowledged by Bogey and Bailly (2010) in the appendix of their paper when they refer to the spurious low frequency noise in their LES-ILEE solution.

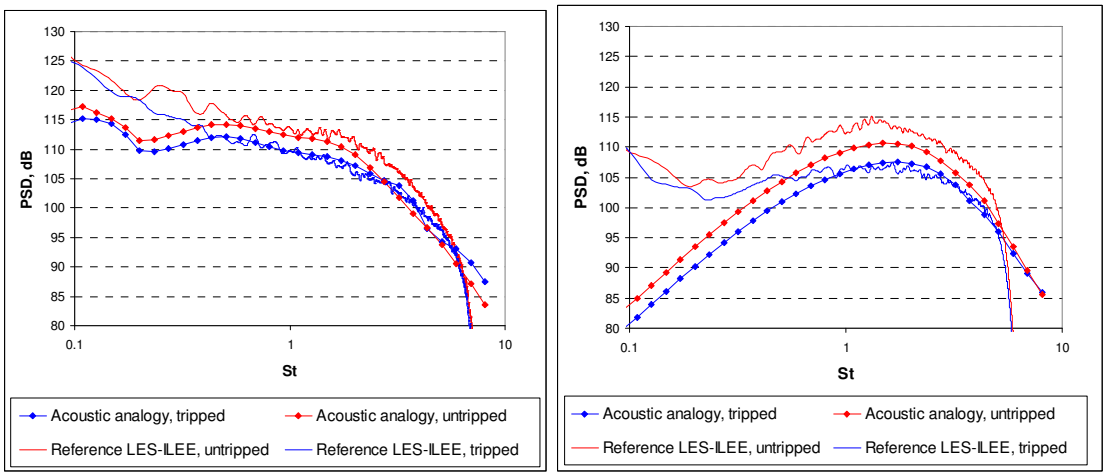

(a) **(b)**

Figure 15. Predicted far-field spectra for (a) 30^0 and (b) 90^0 to the jet axis for the tripped jet and untripped: comparison with the reference LES – ILEE method.

The acoustic analogy model contains three key elements: (i) statistical source model based on the fourth-order velocity correlations that include all significant directivity components, (ii) mean flow sound propagation/interaction through the solution of linearised Euler equations and (iii) non-compact acoustic integration that includes the full source/Green's function convolution in space. For the fully turbulent JEAN jet, Karabasov et al (2010) show that all 3 elements can be crucial for accurate sound predictions. The same check is repeated here for the tripped jet.

Fig.16a,b compares the result of the locally parallel jet approximation with the full linearised Euler propagation model for different angles to the jet. While at 90^0 the difference is insignificant, at 30^0 the error due to neglecting the meanflow - source interference effects due to jet spreading can be as large as 5dB for high frequencies and 8dB for low frequencies. Fig.16c compares the result of full integration result with the "compact" approximation, i.e., the approximation that neglects the source variation in the radial direction in comparison with the propagation scale and that reduces the full convolution to a single space integration. The error due to the compact scales approximation is not as marked as that due to using the locally parallel model, it is within 3-4dB and for many frequencies is less than 2dB. For the same compact model, Fig.16d compares the result of the full source model based on 7 anisotropic components with the statistically isotropic model that assumes certain symmetry of the 4-th order correlation tensor components. For the present initially laminar jet case, the isotropic approximation leads to a 5dB error in sound pressure levels.

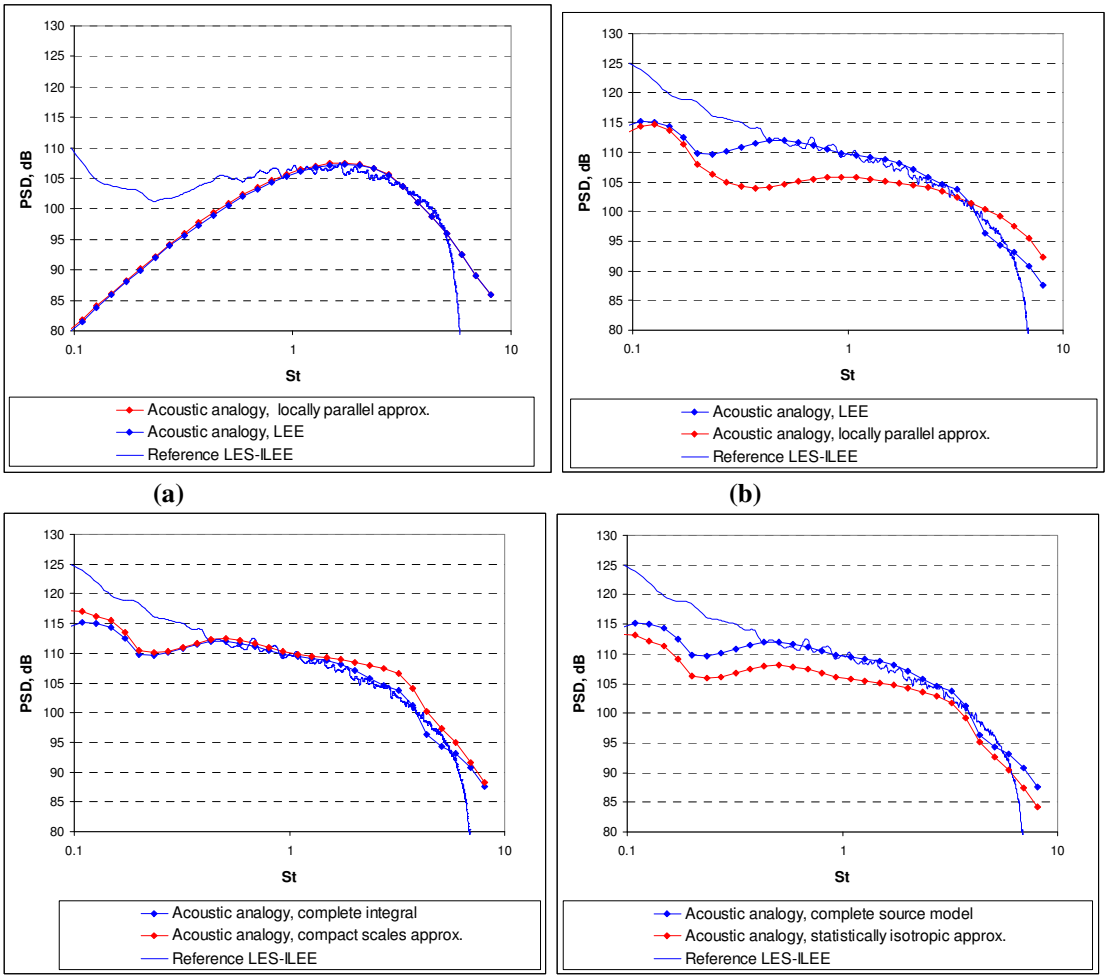

Figure 16. Effect of the locally parallel jet approximation at (a) 90^0 and (b) 30^0 to the jet. (c) Effect of assuming compact integral scales and (d) statistically isotropic source.

VII. Noise sources

One of the main advantages of the acoustic analogy method is that it provides information about the location of efficiently radiating acoustic sources in the jet. The efficient noise source data include both the noise generation mechanisms R_{ijkl} obtained from LES and the propagation term $\hat{I}_{ij}\hat{I}_{kl}$ which accounts for the distributed source - mean flow interaction, which can be very important at small angles to the jet. In the following figures, the spatial distribution of the acoustic integrand weighted with the radius is used as an effective noise source density. Its square integral amounts to the power spectral density at the far-field observer location and the local maxima correspond to the dominant noise sources within the jet.

A. Source strength visualization for the tripped and untripped jet

Fig.17 shows the acoustic integrand distribution within the tripped jet (a,c) and untripped (b,d) at 30^0 and 90^0 angle to the jet axis for the characteristic frequency St=1. For each case, the field is normalised by the peak value. In order to estimate the relative source importance with position within the jet, the contribution to the full sound integral of the acoustic sources which are located in the last 2D of the LES spatial domain in the axial direction is computed. A similar exercise for the radial direction involves computing the contribution of the top 0.2D in the radial direction. The results for each jet and 30^0 and 90^0 angles at St=1 are presented in Table 1. This can be compared with Table 2 that shows results just for the tripped case at St=0.3.

As seen from the tables, as far as radial extent is concerned, the major contributions to noise for both the tripped jet and the untripped one are within the region covered by the LES data, with the top 0.2D of this domain contributing less than 5% of the acoustic energy. For the axial extent, the source fields of both jets are very distributed. The importance of the end-of-potential-core area 9-12D is larger for the small observer angle and more important for the tripped jet that has a longer potential core size. For low frequency, the acoustic source of the tripped jet becomes more concentrated for the 30^0 angle (compare with Fig.9). This suggests that for low-frequency there is an important source part missing in the 9-12D area of the jet, probably due to LES data convergence issues in this region.

Table 1 Relative contribution of the boundary areas to the acoustic integral at St=1

		St=1, 30^0 angle	St=1, 90^0 angle
Tripped jet	Right 2D	30%	23%
	Top 0.2D	3%	3%
Untripped jet	Right 2D	19%	13%
	Top 0.2D	4%	5%

Table 2. Relative contribution of the boundary areas to the acoustic integral for the tripped case at St=0.3

	St=0.3, 30^0 angle	St=0.3, 90^0 angle
Right 2D	17%	29%
Top 0.2D	1%	2%

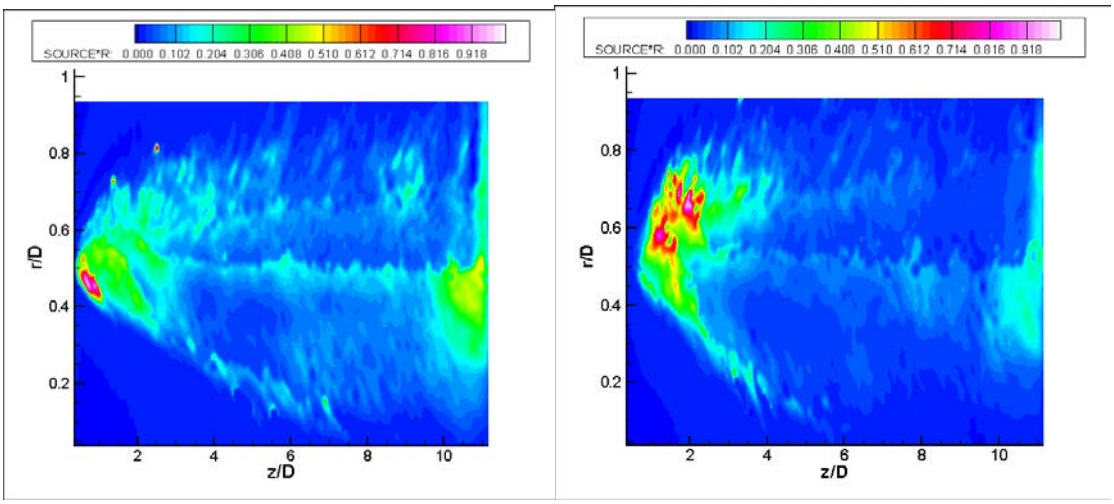

(a) **(b)**

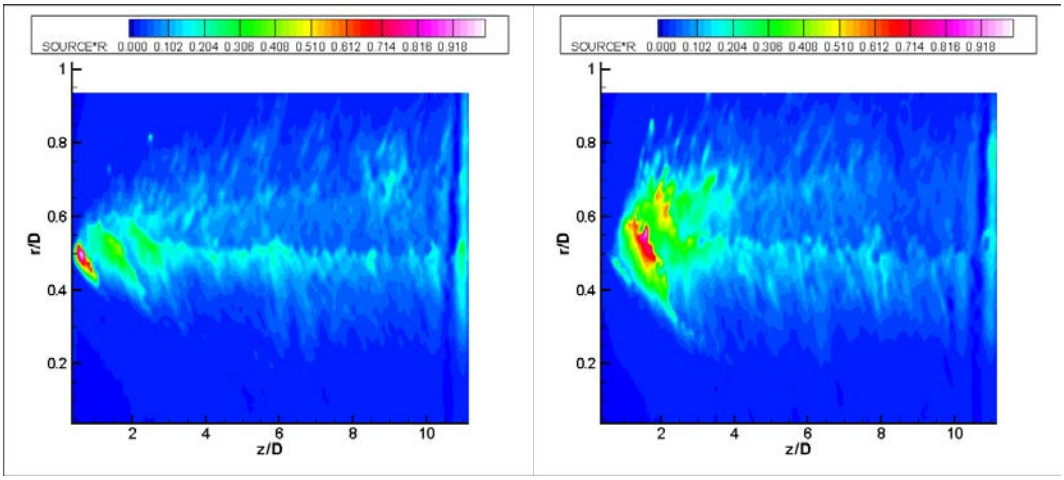

(c) **(d)**

Figure 17. Peak acoustic source location St =1 for (a) tripped jet, observer at 30^0, (b) untripped jet, observer 30^0 (c) tripped jet, observer at 90^0 , (d) untripped jet, observer 90^0 .

It can be seen that the biggest amplitudes of the sources are located at the upstream end of the jet close to the vortex pairing region. Fig.18 shows the efficient source fields of the two jets at 30^0 to the flow that correspond to St=2.16 for the tripped jet case and St=1.61 for the untripped one (the dominant frequencies for the vortex pairing source mechanism identified by Bogey and Bailly). It can be seen that the peak source locations identified here are very similar to those reported in Bogey and Bailly. For the lip-line locations, these are about 0.45D for the tripped jet and 0.8D for the untripped case.

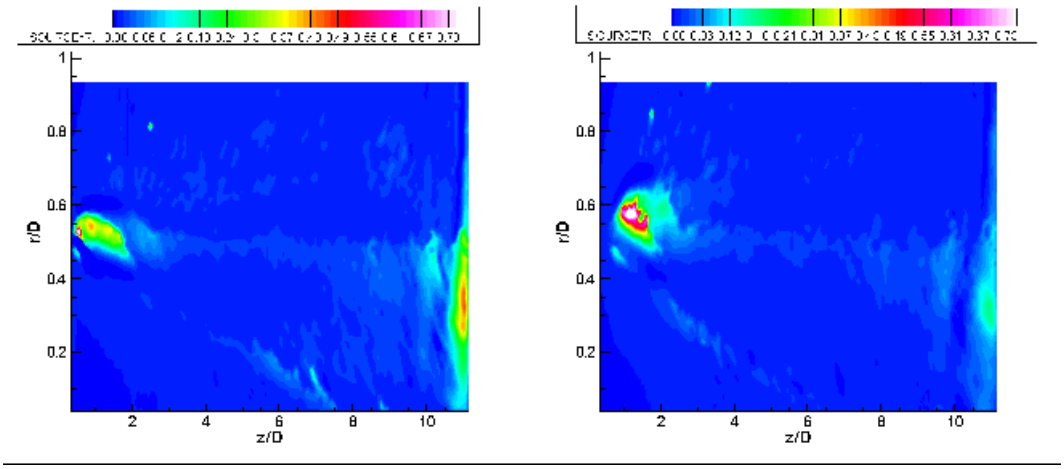

(a) **(b)**

Figure 18. Acoustic sources at the vortex pairing frequency for (a) tripped jet, St = 1.61 and (b) untripped jet, St = 2.16.

B. Contribution of different source length scales to the noise integral

Some insight into which scales are the dominant overall contributor to the radiated noise and which regions of the jet contribute them can be inferred from a decomposition of the source field according to its axial correlation scale. In this section the decomposition of the source spatial density $S(z,r)$ into N non-overlapping ranges S_i each of which corresponds to a particular band of correlation length scales is performed:

$$S(z,r)=\sum_{i=1,N} S_i\ ;\quad S_i = F_i * S(z,r);$$
$$F_i * S(z,r) = S(z,r)\ \text{ if }\ h\cdot(i-1)\le Lz(x,r)\le h\cdot i;\ \text{else}\ F_i * S(z,r)=0; \qquad (5)$$
$$1\le i\le N;\quad h = Max(Lz(x,r))/N.$$

Fig.19 shows several areas of the source S_i for several characteristic scale regions of the tripped jet case considered in Fig.18a. The calculation corresponds to the dominant vortex pairing frequency St=2.16 and 30^0 angle to the flow.

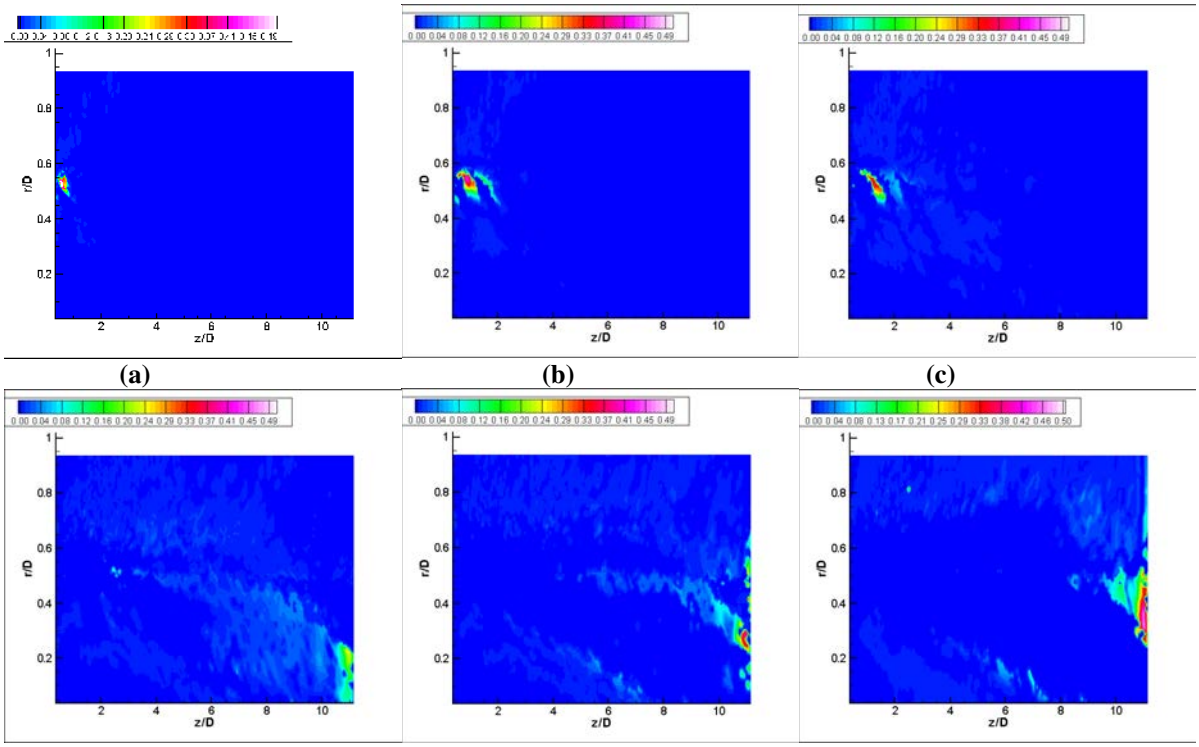

Figure 19. Areas of the efficient acoustic source parts that correspond to particular correlation length scale regions: (a) $0<Lz<0.03D$**, (b)** $0.03D<Lz<0.04D$**, (c)** $0.04<Lz<0.05D$**, (d)** $0.06D<Lz<0.07D$**, (e)** $0.07D<Lz<0.09D$ **and (f)** $Lz>0.09D$**.**

The dominant regions in the first three figures correspond to the early shear layer region in the upstream part of the jet upstream that is typical of the vortex pairing. Those in the last three correspond to the tail of the scale distribution and are associated with jet mixing at the end of the jet potential core (z~ 9D). Fig.20 shows the corresponding acoustic energy budget, i.e., the energy of efficient acoustic sources that is contained in each scale band, $dW/W=\int S_i dzdr \Big/ \int S(x,r)dzdr$. The first local noise maximum is centred around $Lz\sim 0.04D$ that corresponds to the peak noise source close to the location of vortex pairing in the jet. However, this is not a dominant part of the acoustic integral at this frequency for the tripped jet case. The major mechanism contributing to the sound integral comes from the big scales that are located downstream of the end of the jet potential core, $Lz\sim 0.07-0.09D$. Although the local source density amplitudes associated with the big scale locations are 2-3 times smaller than the peak noise associated with the vortex pairing, the area covered by the big scales region is large, making it dominant. This indicates that vortex pairing is not the major noise mechanism at small observer angles in the case of the tripped jet.

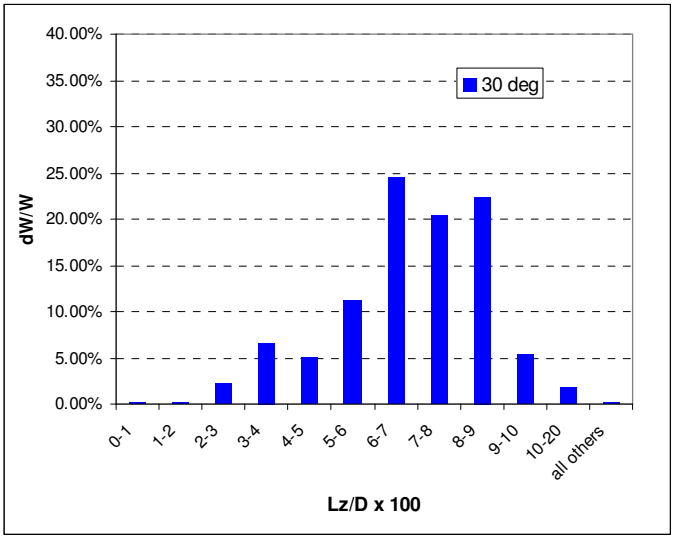

Figure 20. Acoustic energy budget at the vortex pairing frequency for the tripped jet case at 30^0 angle to the flow.

Finally, to investigate the effect of observer angle on the acoustic energy budget the same source decomposition technique (5) is applied for observer angles of 30^0 and 90^0 to the jet and for several frequencies $0.3 < St < 6$. This range corresponds to the range where there is good agreement between the predictions of the acoustic analogy method and the reference LES-ILEE simulation. Fig.21 shows the corresponding acoustic energy budgets.

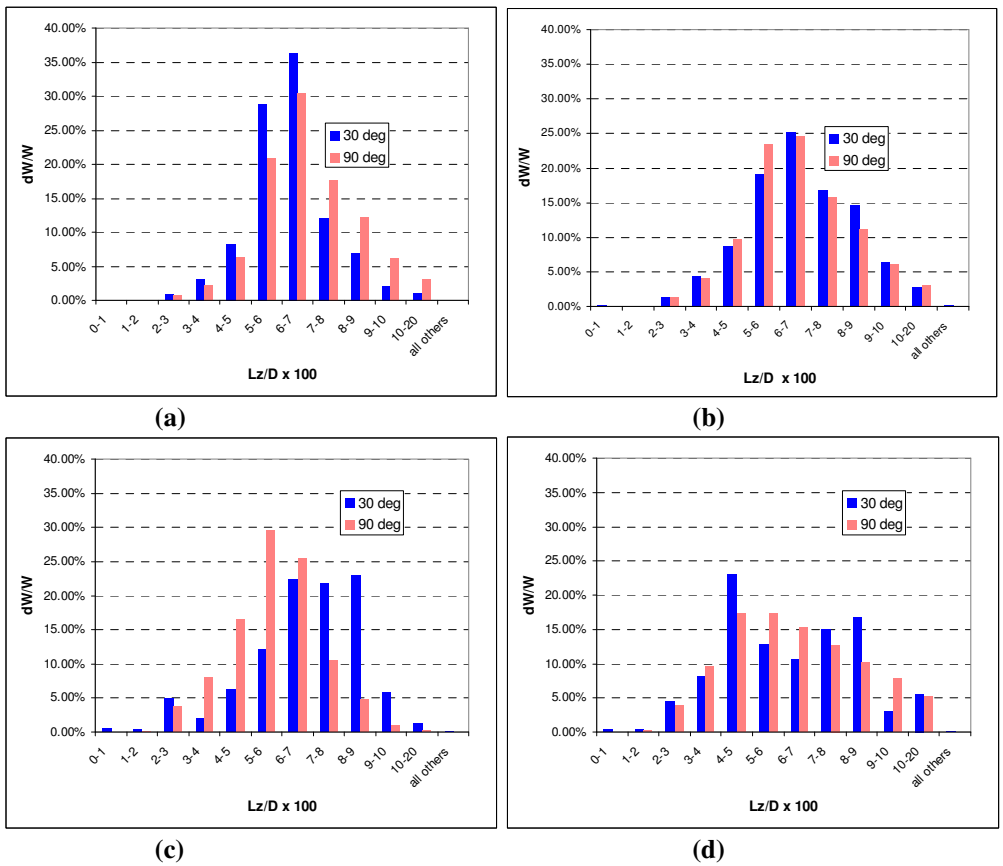

Figure 21. Acoustic energy budget for the tripped jet case at (a) St=0.3, (b) St=1, (c) St=3, (d) St=6.

For the low frequency case, St=0.3, the acoustic energy distribution at 90^0 has significant contributions from a wider range of scales (Fig.21a) when compared with the more peaky small angle case. As frequency is increased, there is a gradual broadening of the contributing range of scales for both angles. For the 30^0 angle to the jet, there is a trend for the acoustic source to be found in 20-30% longer scales when compared to the 90^0 angle. The distributions for 90^0 generally have a single-maximum symmetric profile, with that for high frequencies tending to be centred at the scales close to those of vortex pairing, $Lz \sim 0.04D$. In contrast, for 30^0 a second maximum emerges in the energy distribution. The latter corresponds to the large scale structures at the end of jet potential core of characteristic size $Lz \sim 0.07 - 0.09D$. Despite these differences, the source analysis performed hasn't revealed any significant acoustic energy scale separation depending on the observer angle, e.g., as would have been expected in support for the Fine Scale Source – Large Scale Source theory of Tam at al (2008).

VIII. Conclusion

A modified Goldstein acoustic analogy method using linearised Euler equations and a statistical source model based on Large Eddy Simulation (LES) data has been applied to tripped and untripped, initially-laminar jets. The post-processing of the LES data is performed that and examined critically providing conservative estimates of the areas of the jet which are amenable for the present acoustic analogy model. These areas are the main areas of sound noise generation in the jet potential core including the jet edges and, for high frequencies, the outflow boundary regions just downstream of the end of the potential core.

An attempt was made to fit a Gaussian form to fourth-order correlation statistics and was successful for the vast majority of the area of the jet for which LES statistics were available. Two types of exceptions were noted; one probably due to unconverged statistics in an area of low amplitude and one associated with a "growing and decaying wave" that is typical of the inner edge of the developed shear layer and is more prominent for the untripped jet. Basing on previous experience, the post-processing of the LES fields shows that the credibility limit for the acoustic analogy model predictions at low frequencies is St ~0.2-1.

For both jets, the distribution of correlation source scales is obtained. For the lip-line location, the scales in three spatial directions have similar relative amplitudes, as those found experimentally by Morris and Zaman (2009).

The sound Power Spectral Density predictions of the acoustic analogy model are within 1-2 dB agreement, for the tripped jet, and within 3-4 dB agreement, for the untripped jet, with the reference Large Eddy Simulation - Isotropic Linearied Euler Equations (LES-ILEE) method for 30^0 and 90^0 observer angles to the jet and the frequency range $0.5<St<6$. The less good agreement in the untripped jet case is associated with a strong vortex pairing which is located in the outer shear layers. The discrepancy at high frequencies, $St>6$ between the two methods is likely to be caused by the LES-ILEE surface resolution issues and those for low frequencies, $St<0.5$ could also be associated with the spurious low-frequency noise reported for the original LES-ILEE simulation. For the tripped jet case, the importance of the complete anisotropic statistical source without the isotropy assumption and the full propagation model based on linearised Euler equations is demonstrated. The error due to the non-compact source scales approximation is found to be less severe.

The peak location of efficiently radiating acoustic sources was investigated for the tripped and untripped jets for a few frequencies. The calculated local source strength contours show that the tripped jet has a more extensive source region in comparison with the untripped case, which can be attributed to the differences in the potential core lengths of the jets. For an observer angle of 30^0 to the jet downstream direction, when focusing on the vortex pairing frequency, there are localised sources identified both for the tripped and untripped jets in the early shear layer locations. These locations are close to those reported for the vortex pairing effect in Bogey and Bailly (2010).

A numerical source decomposition technique based on the fourth-order correlation length scales has been used for a detailed investigation of jet noise sources in the tripped jet as a way of attributing sound to different length scales in the jet. For the vortex pairing frequency, there are two types of noise sources found. One, which corresponds to the peak source amplitude, is located at the upstream end of the jet and is associated with the vortex pairing. The other one, which is the dominant source in the acoustic integral, is associated with jet mixing at the end of the jet potential core.

For the tripped jet, the acoustic energy budget as energy distribution per correlation scale band is computed for a wide range of frequencies at 30^0 and 90^0 observer angles. The broadening of energy distribution with frequency is noted. No significant energy scale separation depending on the observer angle is found.

Acknowledgments

The work of SK was supported by the Royal Society of London.

The authors are grateful to Sean Hale for his help in LES data post-processing in the course of a Summer University Research Opportunity Project in Cambridge.

References

[1] Zaman, K.B.M.Q., "Effect of initial condition on subsonic jet noise," AIAA J., Vol. 23, 1985, pp. 1370-1373.

[2] Zaman, K.B.M.Q., "Far-field noise of subsonic jet under controlled excitation," J. Fluid Mech., Vol. 152, 1985, pp. 83-111.

[3] Bogey C. and Bailly C., "Influence of nozzle-exit boundary-layer conditions on the flow and acoustic fields of initially laminar jets", J. Fluid Mech., Vol.663, 2010, pp507-540.

[4] Goldstein, M.E., "A generalized acoustic analogy," J. Fluid Mech., **488**, 2003 pp 315-333.

[5] Karabasov, S.A., Afsar, M.Z., Hynes, T.P., Dowling, A.P., McMullan, W.A., Pokora, C.D., Page, G.J. and McGuirk, J.J.. "Jet Noise - Acoustic Analogy informed by Large Eddy Simulation".AIAA J, 48(7), pp. 1312-1325.

[6] Karabasov, S. A. and Hynes, T. P., "Adjoint Linearized Euler solver in the frequency domain for jet noise modelling," AIAA-2006-2673 12th AIAA/CEAS Cambridge, Massachusetts, 2006.

[7] Power, O., Kerherve, F., Fitzpatrick, J., and Jordan, P., "Measurements of turbulence statistics in high subsonic jets", AIAA-2004-3021, 10th AIAA/CEAS Aeroacoustics Conference, Manchester, UK, June 2004.

[8] Morris P.J. and Zaman K.B.M.Q., "Velocity Measurements in Jets with Application to Noise Source Modeling", Journal of Sound and Vibration, Vol. 329, Issue 4, 15 February 2010, pp. 394-414.

[9] Karabasov, S.A. "Understanding Jet Noise", 'Visions of the future' issue of Phil. Trans. of R.Soc. A: Mathematical, Physical and Engineering Sciences, August 13, 2010, 368, pp.3593-3608.

[10] Tam, C. K. W., Viswanathan, K., Ahuja, K. K. and Panda, J. "The sources of jet-noise: experimental evidence". J. Fluid Mech. 615, 2008, pp. 253–992.